Acta Cryst. (1998). A**54**, 997–1005

Noncentrosymmetric Structure of a Decagonal $Al_{70}Mn_{17}Pd_{13}$ Quasicrystal

Steffen Weber[a,b] and Akiji Yamamoto[a]*

[a]*National Institute for Research in Inorganic Materials, Tsukuba, Ibaraki 305, Japan, and* [b]*Institute of Applied Physics, University of Tsukuba, Tsukuba, Ibaraki 305, Japan. E-mail: yamamoto@nirim.go.jp*

(*Received 18 December 1997; accepted 22 April 1998*)

Abstract

A noncentrosymmetric structure of decagonal $Al_{70}Mn_{17}Pd_{13}$ with the space group $P10_5mc$ was determined for the first time on the basis of a single-crystal X-ray data set. This analysis gave a considerable improvement over the corresponding centrosymmetric model [Weber & Yamamoto (1997). *Philos. Mag.* A**76**, 85–106]. For 1428 independent reflections, $R_w = 0.119$ ($R = 0.167$) and a reasonable chemical composition of $Al_{69.1}Mn_{18.5}Pd_{12.4}$ was obtained by the introduction of the shift from an ideal atom position. The structure loses the inversion center mainly by the breakdown of the mirror plane perpendicular to the tenfold axis which is caused by the asymmetric chemical arrangement.

1. Introduction

The decagonal quasicrystals have a variety of structures with different space groups. They are roughly classified by periods along the tenfold axis. It is known that there are two different structures with a period of about 4 Å in decagonal Al–Co–Ni (*d*-Al–Co–Ni), one of which has the five-dimensional (5D) space group $P10/mmm$ and the other $P10_5/mmc$ (Yamamoto *et al.*, 1990). The former does not have a tenfold screw axis in contrast to the latter. *d*-Al–Pd–Mn and *d*-Al–Mn quasicrystals have a period of about 12 Å (Beeli *et al.*, 1991). These two show similar diffraction patterns consistent with the space group $P10_5/mmc$. They are all centrosymmetric. The first noncentrosymmetric decagonal phase was found in *d*-Al–Ni–Fe. It has been reported that on the Fe-rich side of *d*-Al–Ni–Fe its point group is noncentrosymmetric $\overline{10}m2$ (Saito *et al.*, 1992). Co-rich *d*-Al–Co–Ni also shows similar diffraction patterns, suggesting that these two are isostructural.† Except for this case, all quasicrystals (including the icosahedral one) have been considered to be centrosymmetric. The structure analyses of decagonal quasicrystals made so far are therefore based on the centrosymmetric space groups (Steurer & Kuo, 1990; Steurer *et al.*, 1993; Yamamoto *et al.*, 1990).

Noncentrosymmetric $Al_{70}Ni_{15}Fe_{15}$ has an 8 Å period and is characterized by the existence of a fivefold cluster with 20 Å diameter. As a result, this shows fivefold symmetry in the convergent-beam electron diffraction patterns. This structure is also known as a modulated structure in decagonal quasicrystals. Satellite reflections appear in the odd reciprocal-lattice layers normal to the $\overline{10}$ axis, while there are no satellites in the even layers. It was shown theoretically that such a reflection condition is not explained by a usual 5D space group but by a 5D color group (Yamamoto & Weber, 1997).

On the other hand, *d*-Al–Mn–Pd quasicrystals have been considered to have the centrosymmetric point group of $10/mmm$. Therefore, several structure models with only this symmetry have been proposed (Hiraga *et al.*, 1993; Steurer *et al.*, 1994; Beeli & Horiuchi, 1995; Yamamoto *et al.*, 1995). So far, there has been no attempt to check the possibility of noncentrosymmetric decagonal quasicrystals by X-ray analysis. In a recent paper (Weber & Yamamoto, 1997, referred to as AMP1 hereafter), we presented the results of the refinement of a 5D structure model for the title compound based on 1428 independent reflections [$F \geq 2\sigma(F)$]‡ and on the centrosymmetric space group $P10_5/mmc$. Although this analysis gave a much better result than a former one by Steurer *et al.* (1994), several points still remain unsatisfactory. The R_w factor of 0.16 is not good compared with that of *i*-Al–Pd–Mn (0.10) (Yamamoto *et al.*, 1995). The chemical composition obtained from the refinement was different from the experimental value. An indication for a noncentrosymmetry is the large anisotropic temperature factor for the atoms on the mirror planes perpendicular to the tenfold axis. From these facts, we have already pointed out that the mirror plane normal to the tenfold axis might be broken. Li *et al.* (1992) also suggested the loss of the corresponding mirror plane for its crystal approximant Al_3Mn. The breakdown of the mirror plane leads to the noncentrosymmetric space group $P10_5mc$, which has not been reported yet in any decagonal quasicrystals.

All X-ray analyses of quasicrystals made so far are based on a centrosymmetric model. The present work gives the first detailed analysis of a decagonal quasicrystal based on a noncentrosymmetric space group and clarifies that this gives several improvements over

† A. P. Tsai, private communications.

‡ $I \geq 2\sigma(I)$ in AMP1 should be read as $F \geq 2\sigma(F)$.

ISSN 0108-7673

the results of the former analysis for the centrosymmetric model.

The organization of this paper is as follows. The symmetry is discussed in §2. In §3, the MEM maps are shown. §4 presents the constructed 5D model and the results of the refinement. In §5, the resulting real-space structure is discussed and, in §6, the results are summarized and compared with those of AMP1 and the analysis based on a model by Steurer *et al.* (1994).

2. Symmetry

The symmetry of decagonal quasicrystals is described by a 5D space group since they can be described as crystals in the 5D space. The unit vectors of the decagonal lattice are given by (Yamamoto & Ishihara, 1988)

$$\mathbf{d}_j = (2a/5^{1/2})\{[\cos(2\pi j/5) - 1]\mathbf{a}_1 + \sin(2\pi j/5)\mathbf{a}_2 + [\cos(4\pi j/5) - 1]\mathbf{a}_3 + \sin(4\pi j/5)\mathbf{a}_4\} \quad (j = 1, 2, 3, 4)$$

and $\mathbf{d}_5 = c\mathbf{a}_5 = \mathbf{c}$, where the lattice constants a and c are 2.82 and 12.06 Å (AMP1). The lattice constants of the reciprocal lattice are $a^* = 1/a$ and $c^* = 1/c$. Then the reciprocal unit vectors are

$$\mathbf{d}_j^* = (a^*/5^{1/2})[\cos(2\pi j/5)\mathbf{a}_1 + \sin(2\pi j/5)\mathbf{a}_2 + \cos(4\pi j/5)\mathbf{a}_3 + \sin(4\pi j/5)\mathbf{a}_4] \quad (j = 1, 2, 3, 4)$$

and $\mathbf{d}_5^* = c^*\mathbf{a}_5 = \mathbf{c}^*$. The coordinates x_i and generalized Miller indices h_i ($i \leq 5$) are defined by $\mathbf{x} = \sum_{i=1}^{5} x_i\mathbf{d}_i$ and $\mathbf{h} = \sum_{i=1}^{5} h_i\mathbf{d}_i^*$, where $\mathbf{x}$ and $\mathbf{h}$ are vectors in direct and reciprocal spaces.

The same intensity data as in the refinement of the centrosymmetric model were used (AMP1). The observed systematic extinction ($h_1h_2\overline{h}_2\overline{h}_1h_5$ with $h_5 = 2n + 1$; $0000h_5$ with $h_5 = 2n + 1$) suggests the centrosymmetric $P10_5/mmc$ or noncentrosymmetric $P10_5mc$.

The space group $P10_5mc$ is generated by a tenfold screw axis $\{C_{10}|\mathbf{d}_5/2\}$, a glide plane $\{\sigma'|\mathbf{d}_5/2\}$ parallel to it and lattice translations $\{E|\mathbf{d}_i\}$ ($i \leq 5$). In the format of *International Tables for Crystallography*, these generators are given as $-t, x + y + z + t, -x, -y, u + 1/2$; $-t, -z, -y, -x, u + 1/2$ and lattice translations $1 + x, y, z, t, u$ *etc.*

3. Model building and MEM maps

We employ a cluster model as in AMP1. The initial model is obtained from the centrosymmetric model by removing the mirror planes normal to the tenfold axis which are located at $x_5 = \pm 0.25$. As a result, in the noncentrosymmetric space group, independent occupation domains (ODs) are within $0 \leq x_5 \leq 1/2$, while they are within $0 \leq x_5 \leq 1/4$ in the centrosymmetric case. Therefore more ODs are necessary, which leads to an increase in the number of refinable parameters. Then we get ten ODs which correspond to the finally obtained domains shown in Fig. 1 except for some small parts. (The slight modification of the ODs based on the MEM calculation and the refinement will be mentioned in the next section.) According to our convention, the ODs located at $(i, i, i, i, 5x_5)/5$ ($1 \leq i \leq 5$) are represented by A, B, C, D and E or their lowercase letters. Since the two ODs related by the former mirror plane are no longer equivalent, we distinguish them by primed and unprimed letters. The ODs shown in Fig. 1 give a structure consisting of large columnar 20 Å clusters located at the vertices of a tiling, which is similar to the Penrose pentagon tiling with an edge length of 20 Å. The cluster center positions are generated by a small decagon at the center of OD E. (For the cluster arrangement see Fig. 3 of AMP1.) Other atom positions around the cluster centers are given by the ODs obtained from the OD for cluster centers by shifting it along the external space (Yamamoto *et al.*, 1995; Yamamoto, 1996). In particular, from the OD E a framework pattern with an edge length of about 4.6 Å can be obtained, which harbors different types of

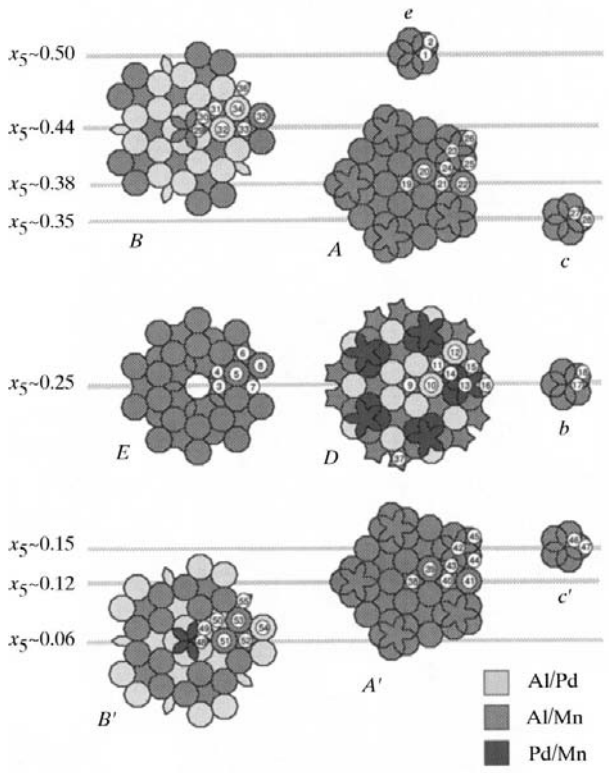

Fig. 1. Constructed ODs (E, e, b, D, A, B, c, A', B', c') for the noncentrosymmetric structure model. The subdomain numbers for the ODs are indicated by labels. The x_5 coordinates for the location of the ODs in the 5D unit cell are also given. The colors light grey, grey and dark grey indicate which pair of elements is assigned to a subdomain.

smaller clusters in the decagonal, pentagonal and star-shaped cages, respectively. This framework is drawn in the external-space MEM maps and the structure projections (Figs. 4 and 6).

In alloys, one atom site is often occupied by two atoms statistically. Since the quasicrystals are usually ternary alloys, the difficulty arises of having to determine a pair of atoms that occupies one site. As shown in AMP1, the MEM is especially efficient to infer the pair. In order to obtain initial phases of reflections necessary for MEM calculations, a noncentrosymmetric model was refined by several cycles with the use of a least-squares program for quasicrystals written by one of the authors (AY). 5D MEM calculations as described in AMP1 were carried out in order to obtain the information necessary to modify the model. They converged to $R_w = 0.030$ ($R = 0.028$). (Unit weights were used.)

Resulting MEM maps showed differences from those in the centrosymmetric model mainly in the peak heights of several domains, which breaks the mirror plane normal to the tenfold axis, although other domains gave similar peak heights. Fig. 2 shows the internal-space MEM maps for the ODs E, e, b, D, c and c', which do not differ significantly from the ones in Fig. 5 of AMP1. Large differences between the two models are, however, found in OD *B*. Fig. 3 shows OD *B* below the former mirror plane on the left side and above it on the right side. The images are arranged in such a way that there would be a mirror relation between the left and right sides for the centrosymmetric case. As can be seen, the electron density is very different especially for $x_5 = 0.05$ *versus* $x_5 = 0.45$, suggesting that the distribution of transition-metal (TM) atoms (Pd atoms in particular) in the OD *B* is quite different compared with the centrosymmetric model.

Subdomains of OD *A* are situated at different heights (x_5 coordinate) as in the centrosymmetric analysis but the x_5 range over which the subdomain extends is different below and above the former mirror plane. (Subdomains extend over $x_5 = 0.07$ to 0.14 and $x_5 = 0.32$ to 0.44.) The MEM maps for the OD *A* are not shown here, since they are similar to Fig. 6 of AMP1.

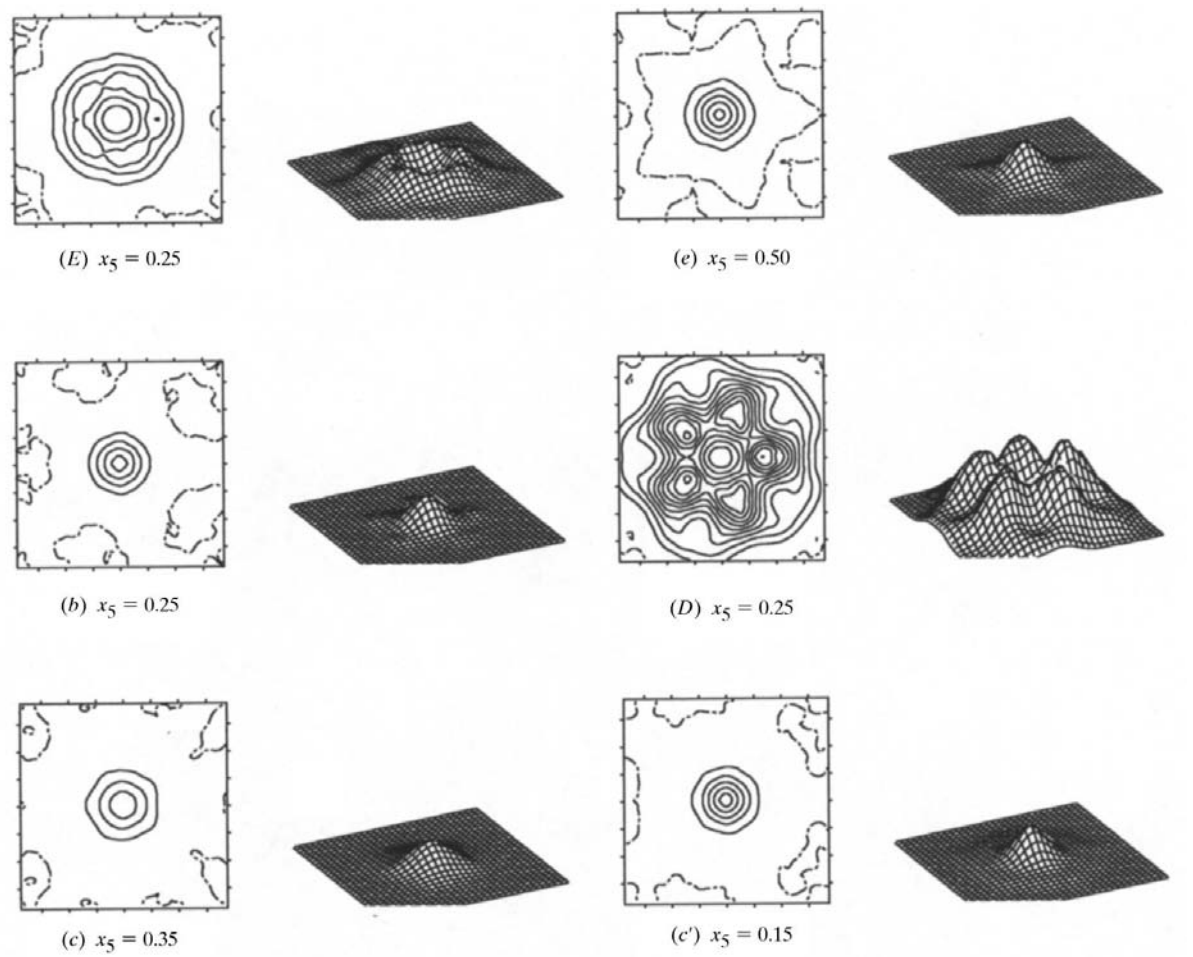

Fig. 2. Internal space MEM maps for the ODs E, e, b, D, c and c'. Note the low electron density at the centers of *E* and *D*. The OD *A* is not shown here, since it extends over a large x_5 range (Fig. 6 in AMP1).

Table 1. *Results of the refinement of the noncentrosymmetric model for decagonal $Al_{70}Mn_{17}Pd_{13}$*

The standard deviation is given in parentheses. The first column lists the numbers of the independent subdomains. The second column gives their internal space shifts $\mathbf{x}^i$. The actual position of the subdomains is then $\mathbf{x}_0 + \mathbf{x}^i$. The superscripts i and e in this table refer to the vector components in the internal and external space, respectively. The displacement along the tenfold axis is given by u_1, while the displacement within the plane normal to the tenfold axis is given by u_2. For u_2, the shift direction $\mathbf{x}_e$ is given. The final atom positions are then obtained by $\mathbf{x} = \mathbf{x}_0 + \mathbf{u}_1[\mathbf{c}/c] + \mathbf{u}_2[\mathbf{x}^e/|\mathbf{x}^e|]$. b_e and b_1 are the isotropic and anisotropic temperature factors. The last column shows the pair of constituent elements assigned to each subdomain. The occupation probability s_1 refers to the second member of those pairs. The element assigned for drawing Fig. 7 is printed in **bold**. In addition to the listed values, a phason temperature factor $b_i = 0.43$ was assigned to all subdomains during the refinement. The first four coordinates of $\mathbf{x}_0$ are clear from the symbol of each OD, that is $\mathbf{x}_0(A/a) = (1, 1, 1, 1, 5x_5)/5$, $\mathbf{x}_0(B/b) = (2, 2, 2, 2, 5x_5)/5$, $\mathbf{x}_0(C/c) = (3, 3, 3, 3, 5x_5)/5$ and $\mathbf{x}_0(D/c) = (4, 4, 4, 4, 5x_5)/5$, while x_5 is listed below ($t = \tau^{-4}$).

sD No.	x^i	x_5	u_1 (Å)	u_2 (Å)	x^e	b_e (Å^{-2})	b_1 (Å^{-2})	s_1	Elements
OD *e*									
1	$(-t, 0, 0, -t, 0, 0)^i$	0.49	0.13 (4)	–		0.00 (2)	0.00 (2)	0.00 (2)	**Al**/Mn
2	$(0, 1, 1, 0, -1, 0)^i$	0.49	−0.02 (6)	–		0.00 (2)	0.00 (2)	0.04 (9)	**Al**/Mn
OD *E*									
3	$(0, -1, -1, 0, 1, 0)^i$	0.25	0.04 (5)	−0.14 (3)	$(0, 1, 1, 0, -1, 0)^e$	0.32 (1)	−0.33 (1)	0.5 (1)	Al/**Mn**
4	$(0, 1, 1, 0, -1, 0)^i$	0.25	0.0 (2)	0.2 (1)	$(0, -1, -1, 0, 1, 0)^e$	0.32 (1)	−0.33(1)	0.00 (2)	**Al**/Mn
5	$(1, 1, 0, -1, -1, 0)^i$	0.25	−0.05 (2)	0.14 (1)	$(1, 1, 0, -1, -1, 0)^e$	0.32 (1)	−0.33 (1)	−0.02 (2)	**Al**/Mn
6	$(0, 0, 0, 0, -1, 0)^i$	0.25	−0.06 (6)	0.57 (4)	$(0, 0, 0, 0, -1, 0)^e$	0.32 (1)	−0.33 (1)	0.00 (2)	**Al**/Mn
7	$(0, 0, 0, 0, 1, 0)^i$	0.25	0.73 (5)	0.26 (6)	$(0, 0, 0, 0, 1, 0)^e$	0.32 (1)	−0.33 (1)	0.00 (2)	**Al**/Mn
8	$(0, -1, 0, 1, 0, 0)^i$	0.25	−0.31 (1)	0.11 (2)	$(0, -1, 0, 1, 0, 0)^e$	0.32 (1)	−0.33 (1)	−0.02 (2)	**Al**/Mn
OD *D*									
9	$(0, 0, 0, 0, 0, 0)^i$	0.25	0.4 (1)	–		−0.01 (1)	0.00 (1)	0.00 (2)	**Al**/Mn
10	$(0, -1, -1, 0, 1, 0)^i$	0.25	−0.07 (1)	−0.17 (0)	$(0, 1, 1, 0, -1, 0)^e$	−0.01 (1)	0.00 (1)	0.65 (2)	Al/**Pd**
11	$(0, 0, -1, -1, 0, 0)^i$	0.25	0.01 (6)	−0.22 (4)	$(0, 0, 1, 1, 0, 0)^e$	−0.01 (1)	0.00 (1)	−0.01 (2)	**Al**/Mn
12	$(-1, 0, 0, 0, 0, 0)^i$	0.25	0.19 (3)	0.08 (4)	$(1, 0, 0, 0, 0, 0)^e$	−0.01 (1)	0.00 (1)	−0.03 (1)	**Al**/Pd
13	$(0, 0, 0, 0, -1, 0)^i$	0.25	−0.02 (1)	0.24 (1)	$(0, 0, 0, 0, 1, 0)^e$	−0.01 (1)	0.00 (1)	0.82 (4)	Pd/**Mn**
14	$(-1, -1, 0, 1, 1, 0)^i$	0.25	−0.04 (1)	−0.12 (1)	$(1, 1, 0, -1, -1, 0)^e$	−0.01 (1)	0.00 (1)	0.00 (2)	**Pd**/Mn
15	$(0, 1, 0, -1, 0, 0)^i$	0.25	0.00 (6)	−0.18 (4)	$(0, -1, 0, 1, 0, 0)^e$	−0.01 (1)	0.00 (1)	0.00 (2)	**Al**/Mn
16	$(0, -1, -1, 0, 2, 0)^i$	0.25	0.07 (5)	−0.17 (5)	$(0, 1, 1, 0, -2, 0)^e$	−0.01 (1)	0.00 (1)	0.09 (7)	**Al**/Pd
37	$(-1, 0, 1, -1, -1, 0)^i$	0.25	−0.09 (2)	0.05 (2)	$(0, 1, 1, 0, -1, 0)^e$	−0.01 (1)	0.43 (5)	0.49 (8)	**Al**/Mn
OD *b*									
17	$(-t, 0, 0, -t, 0, 0)^i$	0.25	0.01 (3)	–		0.42 (3)	0.42 (3)	0.00 (2)	**Al**/Mn
18	$(0, 1, 1, 0, -1, 0)^i$	0.25	0.01 (3)	−0.1 (1)	$(0, -1, -1, 0, 1, 0)^e$	0.42 (3)	0.42 (3)	0.00 (2)	**Al**/Mn
OD *A*									
19	$(0, 0, 0, 0, 0, 0)^i$	0.37	−0.3 (1)	–		0.00 (3)	0.00 (3)	0.00 (2)	**Al**/Mn
20	$(0, 1, 1, 0, -1, 0)^i$	0.39	0.28 (2)	0.04 (4)	$(0, 1, 1, 0, -1, 0)^e$	−0.01 (3)	−0.01 (3)	−0.01 (2)	**Al**/Mn
21	$(0, 0, 1, 1, 0, 0)^i$	0.39	0.39 (7)	−0.08 (5)	$(0, 0, 1, 1, 0, 0)^e$	0.68 (3)	−0.68 (4)	−0.01 (2)	**Al**/Mn
22	$(1, 0, 0, 0, 0, 0)^i$	0.37	−0.12 (3)	−0.06 (4)	$(1, 0, 0, 0, 0, 0)^e$	1.7 (5)	0.1 (8)	0.4 (1)	**Al**/Mn
23	$(0, 0, 0, 0, -1, 0)^i$	0.39	0.23 (2)	−0.01 (2)	$(0, 0, 0, 0, -1, 0)^e$	−0.01 (3)	0.00 (3)	−0.01 (2)	**Al**/Mn
24	$(1, 1, 0, -1, -1, 0)^i$	0.37	−0.02 (1)	0.18 (2)	$(1, 1, 0, -1, -1, 0)^e$	0.00 (2)	0.00 (3)	1.00 (2)	Al/**Mn**
25	$(0, -1, 0, 1, 0, 0)^i$	0.39	−0.14 (9)	−0.01 (8)	$(0, -1, 0, 1, 0, 0)^e$	2. (1)	−1. (2)	0.00 (2)	**Al**/Mn
26	$(0, 1, 1, 0, -2, 0)^i$	0.39	−0.23 (3)	0.22 (4)	$(0, 1, 1, 0, -2, 0)^e$	0.4 (4)	−0.4 (7)	1.00 (2)	Al/**Mn**
OD *c*									
27	$(t, 0, 0, t, 0, 0)^i$	0.35	0.0 (1)	–		0.27 (3)	0.27 (3)	0.00 (2)	**Al**/Mn
28	$(0, -1, -1, 0, 1, 0)^i$	0.35	0.01 (8)	–		0.27 (3)	0.27 (3)	0.3 (2)	**Al**/Mn
OD *B*									
29	$(-t, 0, 0, -t, 0, 0)^i$	0.45	−0.2 (1)	0.17 (6)	$(-1, 0, 0, -1, 0, 0)^e$	0.45 (1)	−0.46 (4)	0.8 (6)	Al/**Mn**
30	$(0, 1, 1, 0, -1, 0)^i$	0.45	−0.17 (3)	−0.10 (2)	$(0, -1, -1, 0, 1, 0)^e$	0.45 (1)	0.4 (2)	1.0 (2)	Al/**Pd**
31	$(0, 0, 1, 1, 1, 0)^i$	0.45	−0.28 (7)	0.09 (7)	$(0, 0, 1, 1, 1, 0)^e$	0.45 (1)	0.45 (4)	0.00 (2)	**Al**/Mn
32	$(1, 0, 0, 0, 1, 0)^i$	0.45	−0.12 (2)	−0.04 (2)	$(1, 0, 0, 0, 1, 0)^e$	0.45 (1)	0.47 (4)	0.40 (7)	**Al**/Pd
33	$(0, 0, 1, 0, 0, 0)^i$	0.45	−0.25 (4)	−0.35 (4)	$(0, 0, 1, 0, 0, 0)^e$	0.45 (1)	−0.45 (4)	0.2 (2)	**Al**/Mn
34	$(-1, 0, 2, 1, 0, 0)^i$	0.43	−0.03 (1)	0.05 (1)	$(-1, 0, 2, 1, 0, 0)^e$	0.45 (1)	0.46 (4)	0.40 (3)	**Al**/Pd
35	$(1, 1, 1, -1, 0, 0)^i$	0.45	−0.16 (1)	0.21 (1)	$(1, 1, 1, -1, 0, 0)^e$	0.45 (1)	−0.2 (2)	1.00 (2)	Al/**Mn**
36	$(1, -1, -1, 1, 1, 0)^i$	0.45	−0.18 (2)	0.40 (2)	$(1, -1, -1, 1, 1, 0)^e$	0.45 (1)	−0.46 (4)	0.8 (1)	Al/**Pd**
OD *A′*									
38	$(0, 0, 0, 0, 0, 0)^i$	0.13	0.2 (2)	–		1.34 (4)	1.34 (4)	0.00 (2)	**Al**/Mn
39	$(0, 1, 1, 0, -1, 0)^i$	0.11	0.13 (1)	0.15 (1)	$(0, 1, 1, 0, -1, 0)^e$	−0.02 (3)	−0.01 (3)	0.8 (1)	Al/**Mn**
40	$(0, 0, 1, 1, 0, 0)^i$	0.11	−0.05 (6)	0.11 (5)	$(0, 0, 1, 1, 0, 0)^e$	0.32 (4)	−0.32 (4)	0.00 (2)	**Al**/Mn
41	$(1, 0, 0, 0, 0, 0)^i$	0.13	−0.45 (3)	0.24 (3)	$(1, 0, 0, 0, 0, 0)^e$	0.35 (4)	−0.35 (4)	−0.01 (2)	**Al**/Mn
42	$(0, 0, 0, 0, -1, 0)^i$	0.11	0.10 (2)	0.18 (3)	$(0, 0, 0, 0, -1, 0)^e$	0.00 (3)	0.00 (3)	−0.01 (2)	**Al**/Mn
43	$(1, 1, 0, -1, -1, 0)^i$	0.13	−0.51 (4)	0.03 (6)	$(1, 1, 0, -1, -1, 0)^e$	0.00 (3)	0.00 (3)	−0.01 (2)	**Al**/Mn
44	$(0, -1, 0, 1, 0, 0)^i$	0.11	−0.02 (3)	0.11 (4)	$(0, -1, 0, 1, 0, 0)^e$	0.55 (3)	−0.55 (4)	0.5 (2)	Al/**Mn**
45	$(0, 1, 1, 0, -2, 0)^i$	0.11	0.32 (6)	0.26 (9)	$(0, 1, 1, 0, -2, 0)^e$	2. (1)	1. (2)	0.6 (4)	Al/**Mn**
OD *c′*									
46	$(t, 0, 0, t, 0, 0)^i$	0.15	0.10 (5)	–		0.00 (2)	0.00 (2)	0.00 (2)	**Al**/Mn
47	$(0, -1, -1, 0, 1, 0)^i$	0.15	−0.06 (5)	–		0.00 (2)	0.00 (2)	0.00 (2)	**Al**/Mn

Table 1 (*cont.*)

sD No.	x^i	x_5	u_1 (Å)	u_2 (Å)	x^e	b_e (Å^{-2})	b_1 (Å^{-2})	s_1	Elements
OD B'									
48	$(-t, 0, 0, -t, 0, 0)^i$	0.05	−0.02 (1)	0.02 (9)	$(-1, 0, 0, -1, 0, 0)^e$	0.07 (1)	0.07 (4)	0.2 (1)	**Pd**/Mn
49	$(0, 1, 1, 0, -1, 0)^i$	0.05	0.07 (4)	0.23 (2)	$(0, -1, -1, 0, 1, 0)^e$	0.07 (1)	−0.07 (4)	0.38 (9)	**Al**/Pd
50	$(0, 0, 1, 1, 1, 0)^i$	0.05	0.18 (1)	0.00 (1)	$(0, 0, 1, 1, 1, 0)^e$	0.07 (1)	0.09 (4)	1.00 (2)	Al/**Pd**
51	$(1, 0, 0, 0, 1, 0)^i$	0.05	0.14 (6)	−0.11 (4)	$(1, 0, 0, 0, 1, 0)^e$	0.07 (1)	0.08 (4)	0.00 (2)	**Al**/Mn
52	$(0, 0, 1, 0, 0, 0)^i$	0.05	−0.02 (3)	0.12 (3)	$(0, 0, 1, 0, 0, 0)^e$	0.07 (1)	0.07 (4)	0.5 (2)	Al/**Mn**
53	$(-1, 0, 2, 1, 0, 0)^i$	0.07	−0.12 (3)	−0.08 (2)	$(-1, 0, 2, 1, 0, 0)^e$	0.07 (1)	0.07 (4)	−0.01 (2)	**Al**/Mn
54	$(1, 1, 1, -1, 0, 0)^i$	0.05	0.05 (1)	−0.38 (1)	$(1, 1, 1, -1, 0, 0)^e$	0.07 (1)	0.07 (4)	0.23 (2)	**Al** /Pd
55	$(1, -1, -1, 1, 1, 0)^i$	0.05	0.20 (3)	−0.07 (2)	$(1, -1, -1, 1, 1, 0)^e$	0.07 (1)	−0.0 (4)	1.0 (1)	Al/**Pd**

Fig. 4 shows an external space MEM map for a 50×50 Å range corresponding to a structure projection along the tenfold axis. The positions labeled A, B and C indicate some interesting features which will be discussed in §5 in the light of this new noncentrosymmetric structure model.

4. Five-dimensional structure model and refinement

As shown in Fig. 1, there are 55 independent subdomains, for each of which the shift from the ideal position, temperature factor and occupation probability can be defined. The locations of the centers of the independent subdomains are given in Table 1 by $\mathbf{x}_0 + \mathbf{x}^i$.

Analogous to AMP1, the following parameters were refined using the least-squares method: s_1 occupation probability of the second member of a pair element1/element2 assigned to a subdomain (the occupation probability of the first member is then $s_0 = 1 - s_1$); b_e isotropic temperature factor; b_1 anisotropic temperature factor; u_1 atom shift along the tenfold axis; u_2 atom shift perpendicular to the tenfold axis; b_i phason temperature factor. Furthermore, three penalty functions PF_1, PF_2 and PF_3 were used to maintain the occupation probability, temperature factor and chemical composition within reasonable ranges. (For their expressions, see AMP1.) From the peak heights in the MEM maps, pairs of elements occupying the subdomains are chosen.

The present model leads to many parameters, so that we tried to refine some parameters commonly for a group of subdomains, in order to keep the number of parameters smaller. This worked fine for the refinement of b_e and b_1 for the ODs E, e, D, b, c and c'. However, for the other ODs (A, A', B, B') an improvement was only obtained by individually refining all parameters for each subdomain. The gradients for the three penalty functions PF_1, PF_2 and PF_3 were chosen to be 0.5, 0.3 and 0.3, respectively.

After several modifications of the ODs and pairs of elements for each subdomain, we finally get $R_w = 0.119$ ($R = 0.167$) for 1428 reflections. (The weighting scheme is defined in AMP1.) In Table 1, all refined parameters are listed for the noncentrosymmetric model of decagonal $Al_{70}Mn_{17}Pd_{13}$. In addition to the listed values, a phason temperature factor, which is common to all subdomains, was refined to be $b_i = 0.43$. Quite large shifts along the tenfold axis resulted for the subdomains 7, 41, 43 and perpendicular to it for the subdomains 6 and 36. Furthermore, some temperature factors are still high for the ODs A and A' (22, 25, 38, 45). Fig. 5 shows the final fit for the refinement. The point density for the present model is the same as for the centrosymmetric model, namely 0.0677 Å^{-3}. The refined chemical composition is $Al_{69.1}Mn_{18.5}Pd_{12.4}$.

5. Real-space structure and cluster types

The structure of decagonal quasicrystals can be regarded as a layer structure. In the present case, atom layers normal to the tenfold axis are grouped roughly into ten layers, although all the layers are puckered because of the loss of the mirror plane. The resulting stacking sequence of ten layers can be written as $(e + \mathbf{e}')$ $\mathbf{B}'$ $(\mathbf{A}' + \mathbf{c}')$ $(\mathbf{E} + \mathbf{D} + \mathbf{b})$ $(\mathbf{A} + \mathbf{c})$ $\mathbf{B}$ $(\mathbf{e} + e')$ C' $(D' + b')$ $(E + A + c)$ $(D + b)$ C, whereby the independent part is printed in bold letters. The letters characterizing a given layer correspond to the ODs that create the atoms of that layer. Fig. 6 shows the projected structure of the refined model along the tenfold axis. The structure consists of four cluster types labelled 1–4. Among them, only the last one is seen in the crystal approximant Al_3Mn (Hiraga *et al.*, 1993; Hiraga & Sun, 1993). Fig. 7 shows the four cluster types. Al-rich sites are drawn as white atoms and TM-rich sites as black atoms with the exception of the site for 35, which is drawn in grey, since this atom was refined as a transition-metal atom but its electron density in Fig. 4 is quite low.

Very interesting are the features at the two positions labelled A and B (indicated by arrows in Fig. 6). The atoms at A are generated by the subdomains 36 and 55. In the centrosymmetric model, this site was only due to 36. In AMP1, we discussed the difficulty of explaining the split-atom position for this subdomain as found in the external space MEM map (see atom position B in Fig. 4). This noncentrosymmetric model, however, gives a very simple explanation for this feature. The site at A

shows two slightly split atom positions. One results from 36 and the other from 55.

The site at *B* shows four atom positions. In the centrosymmetric model, there were only two resulting from the subdomain 35. In this noncentrosymmetric model, they come from 35 (refined as TM) and 54 (refined as Al). From this, one should assume a clearer electron density for 35 in the external space MEM map, which also displays the feature of split positions for these subdomains. In Fig. 4, the corresponding atom positions are indicated by the label *C*. Looking at all equivalent positions in the five large clusters shown, we

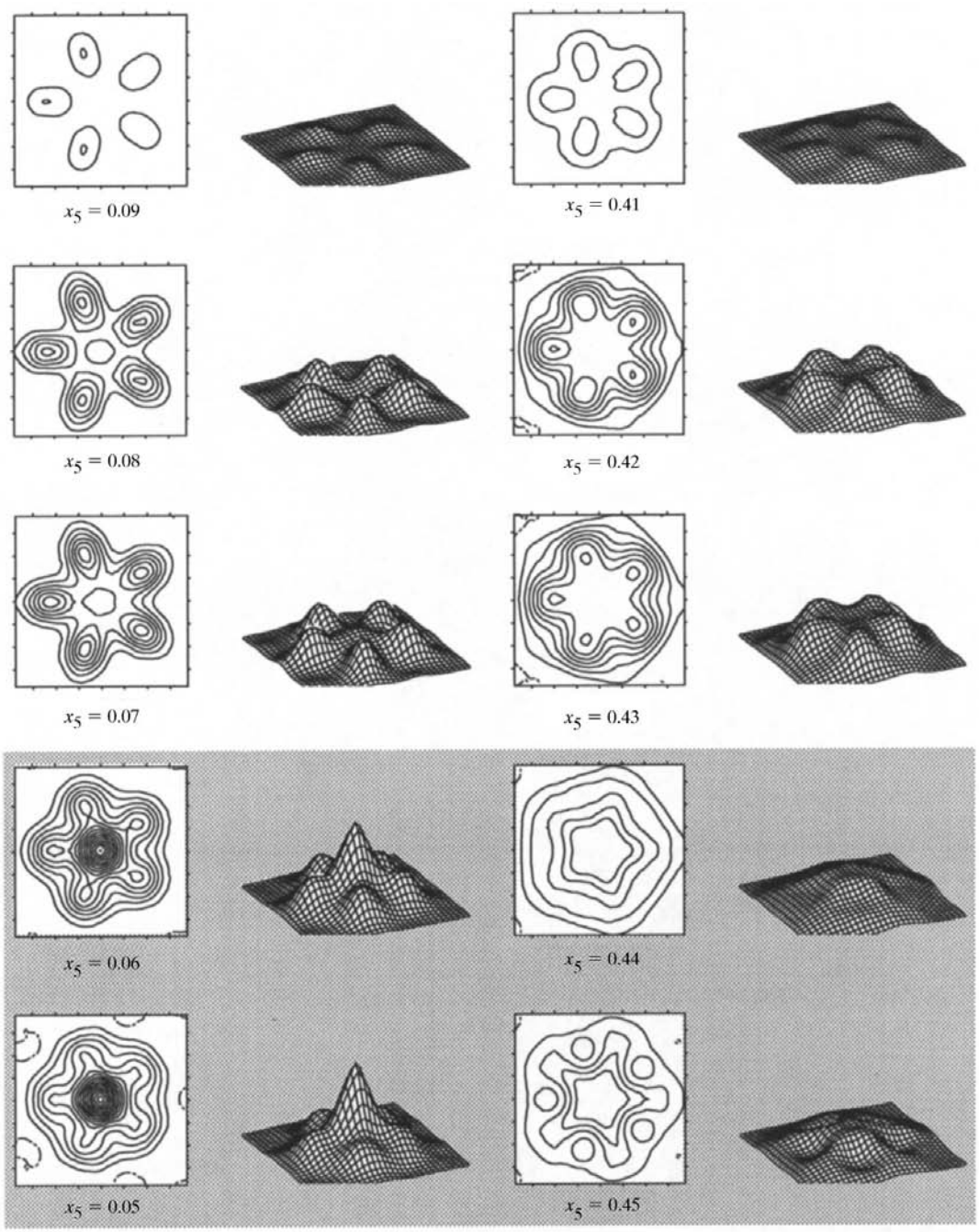

Fig. 3. Internal space MEM maps for the OD *B* at different x_5 levels within the asymmetric unit cell, which extends from $x_5 = 0.0$ to 0.5. For the centrosymmetric space group, there would be a mirror relation between the plots on the left and on the right. Especially from the plots within the shaded rectangle, it is clear that this relation is broken for the noncentrosymmetric case.

Table 2. *Comparison of results of the refinements for the centrosymmetric (AMP1) and noncentrosymmetric structure models*

Model	Centrosymmetric	Noncentrosymmetric
Parameters	121	217
R_w (R), 1428 reflections	0.157 (0.234)	0.119 (0.167)
R_w (R), 500 reflections	0.129 (0.129)	0.093 (0.096)
Chemical composition	$Al_{61.4}Mn_{20}Pd_{18.6}$	$Al_{69.1}Mn_{18.5}Pd_{12.4}$
Point density	0.0677	0.0677
Space group	$P10_5/mmc$	$P10_5mc$

indeed see that the density for 35 is sometimes more distinct than for 54 (see shaded circles in Fig. 4).

6. Concluding remarks and discussion

The model with the noncentrosymmetric space group $P10_5mc$ for d-$Al_{70}Mn_{17}Pd_{13}$ gave an improved R factor, calculated chemical composition, and a natural interpretation of the split-atom positions observed in the MEM map of AMP1. The results of the former analysis of the centrosymmetric model and the present one are summarized in Table 2.

Compared to the centrosymmetric model, the R_w factor dropped by about 0.04 and the R factor by about 0.07. Comparison of Fig. 5 with Fig. 8 of AMP1 reveals that the improved fit mainly affects the bulk of weak reflections, whereas the fit for the strongest reflections did not improve much. The chemical composition is much closer to the true composition ($Al_{70}Mn_{17}Pd_{13}$) than the one obtained for the centrosymmetric model. The results clearly indicate that the noncentrosymmetric space group has to be favored for the description of the structure of decagonal Al–Mn–Pd quasicrystals.

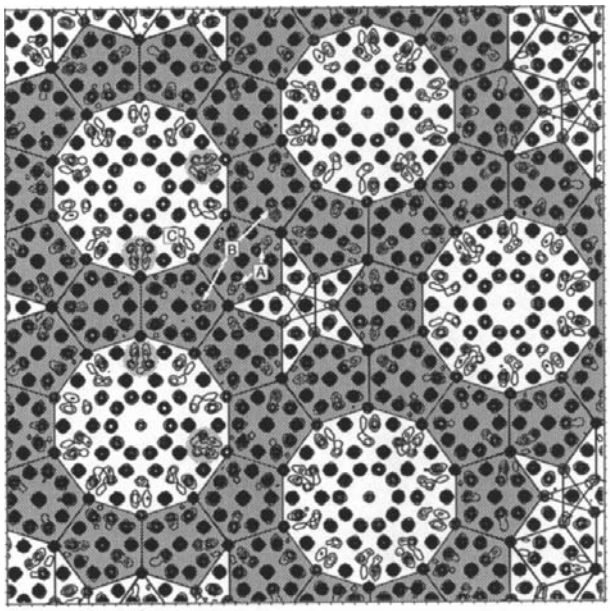

Fig. 4. External space MEM map (50 × 50 Å) for d-$Al_{70}Mn_{17}Pd_{13}$ obtained from the $h_1h_2h_3h_40$ reflections only (identical to Fig. 7 in AMP1). The features at the positions labelled *A*, *B* and *C* are discussed in the text.

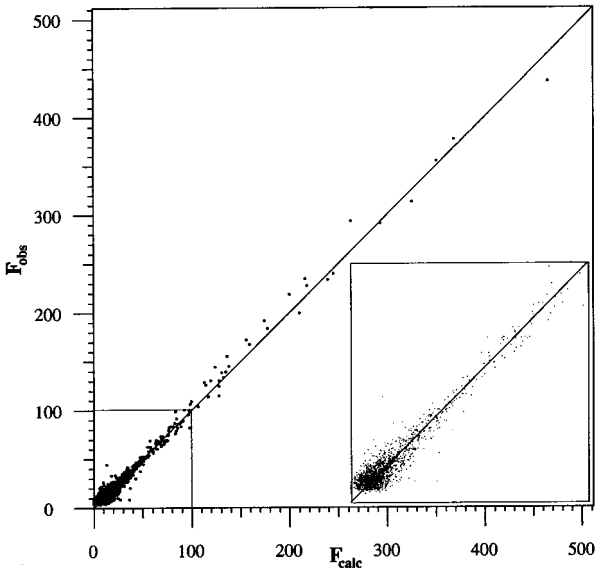

Fig. 5. Final fit for the refinement of the noncentrosymmetric model. The F_{obs} are plotted against the absolute values of the F_{calc}. The bulk of weak reflections ($|F_{calc}| < 100$) shows a better fit compared with Fig. 8 in AMP1.

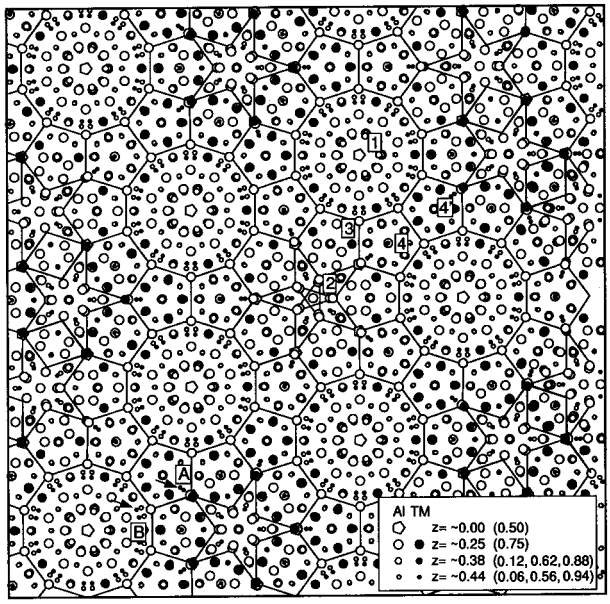

Fig. 6. Structure projection of the noncentrosymmetric model along the tenfold axis. The different cluster types are labelled 1–4. As explained in the text, the split-atom positions at the points labelled *A* and *B* (indicated by arrows) seem to explain more naturally the corresponding electron density in the external space MEM map in Fig. 4.

Our previous model in AMP1 already gave a better R_w factor than that of Steurer *et al.* but the data set used is different. In order to confirm that the cluster model employed by us is better than older models, we refined their model by using the present data set and obtained $R_w = 0.22$ for the strongest 500 reflections. This is comparable with the value $R_w = 0.21$ for 476 reflections in the original paper (Steurer *et al.*, 1994), indicating that the difference in the R_w factors is coming from the models. This shows clearly that in order to obtain better results the use of the cluster model is necessary and the refinement of the cluster structure is essentially important for a quasicrystal structure analysis.

The present analysis is however still not complete. As seen in Table 1, some anisotropic temperature factors are very small. In order to check whether they are due to an inclusion of the diffuse scattering intensities, the refinement was repeated for a subset of the data with $F \geq 10\sigma(F)$ (624 reflections), since mainly the weak reflections would be affected by such a contribution to their intensities. However, no change in the temperature factors could be observed. The difference Fourier map showed a maximum difference of 5.5% of the scattering power of Al ($\Delta\rho_{\min} = -8.9$ and $\Delta\rho_{\max} = 9.6$ e Å^{-3}). These peak densities are not small enough in the sense of the usual crystal structure analysis. Peaks in the map appear in the OD's *D* (mainly TM, around 10 and 13) and near the boundaries of the OD's B (mainly TM, around 36 and 55) and *A* (mainly Al, around 22). The former means that a finer subdivision of the OD *D* may

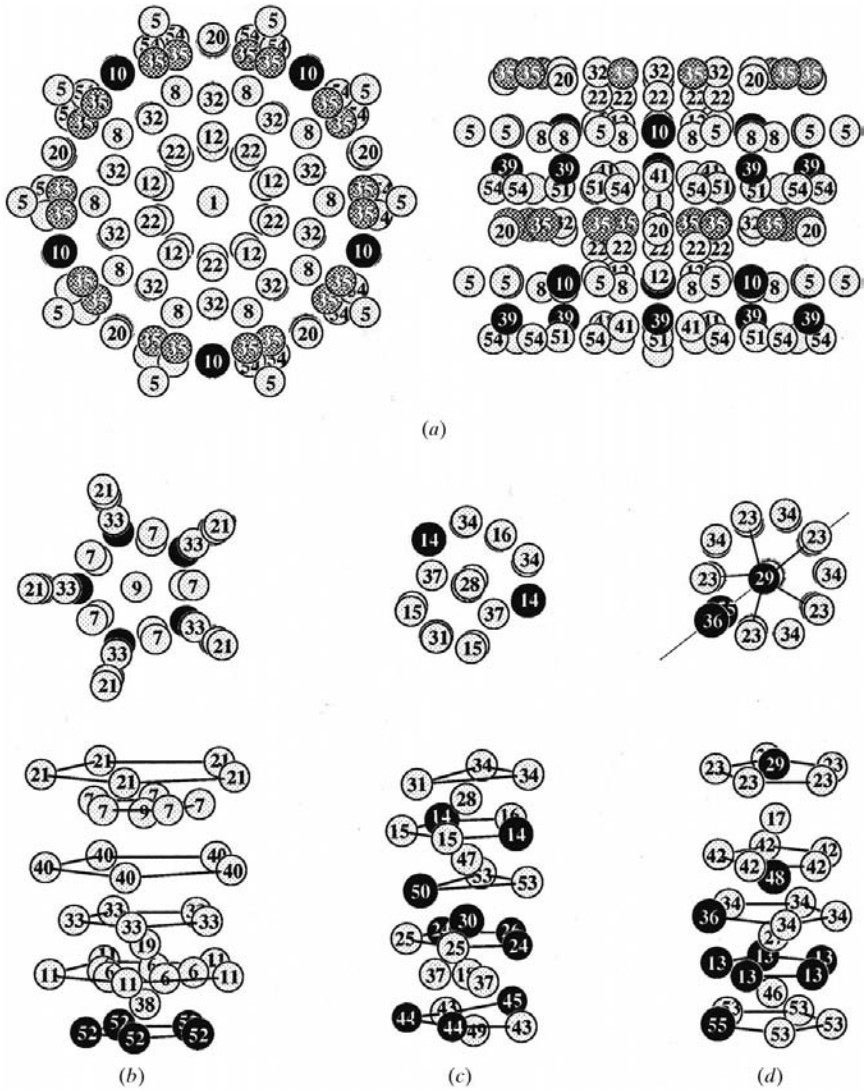

Fig. 7. The four types of columnar clusters for the noncentrosymmetric structure model of $Al_{70}Mn_{17}Pd_{13}$ in a top view and a side view. (*a*), (*b*), (*c*), (*d*) correspond to clusters 1, 2, 3, 4 in Fig. 6. Al-rich sites are drawn as white atoms and TM-rich sites as black or grey atoms. An explanation for the grey atoms (35) is given in the text.

give a better result but it introduces more parameters, which makes the analysis difficult, while the latter may indicate some disordering by the phason flip.

The external space MEM maps seem to provide valuable information, which may aid the choice of either a centrosymmetric or a noncentrosymmetric structure model, provided that suitable split-atom positions are present. On the other hand, MEM maps generally depend on the choice of the phases of reflections. This means that they do not always give a correct result. In the present study, we met an inconsistency between the results of MEM calculations and refinements for the shapes of the ODs B and B'. In our experience, the MEM tends to give a too small density for a lower-density region and a too high density for the peak. One must therefore check the density given by the MEM by the refinement as we did.

The authors thank Dr M. Onoda, NIRIM, for valuable discussions. The sample of d-Al–Mn–Pd used in the present study was supplied by Professor Y. Matsuo, Nara Womens University. This work is partially supported by 'Core Research for Evolutional Science and Technology'. One of the authors (SW) thanks Professor K. Ohshima, University of Tsukuba, for encouragement in the course of the present work.

References

Beeli, C. & Horiuchi, S. (1995). *Aperiodic '94*, edited by G. Chapuis & W. Paciorek, pp. 356–360. Singapore: World Scientific.

Beeli, C., Nissen, H. U. & Robadey, J. (1991). *Philos. Mag. Lett.* **63**, 87–95.

Hiraga, K., Kaneko, M., Matsuo, Y. & Hashimoto, S. (1993). *Philos. Mag.* B**67**, 193–205.

Hiraga, K. & Sun, W. (1993). *Philos. Mag. Lett.* **67**, 117–123.

Hiraga, K., Sun, W., Lincoln, F. J. & Matsuo, Y. (1993). *Phase Transit.* **44**, 163–172.

Li, X. Z., Shi, D. & Kuo, H. (1992). *Philos. Mag.* B**66**, 331.

Saito, M., Tanaka, M., Tsai, A. P., Inoue, A. & Masumoto, T. (1992). *J. Appl. Phys.* **31**, L109–L112.

Steurer, W., Haibach, T., Zhang, B., Beeli, C. & Nissen, H. U. (1994). *J. Phys. Condens. Matter*, **6**, 613–632.

Steurer, W., Haibach, T., Zhang, B., Kek, S. & Lück, R. (1993). *Acta Cryst.* B**49**, 661–675.

Steurer, W. & Kuo, H. K. (1990). *Acta Cryst.* **46**, 703–712.

Weber, S. & Yamamoto, A. (1997). *Philos. Mag.* A**76**, 85–106.

Yamamoto, A. (1996). *Acta Cryst.* A**52**, 509–560.

Yamamoto, A. & Ishihara, K. N. (1988). *Acta Cryst.* A**44**, 707–714.

Yamamoto, A., Kato, K., Shibuya, T. & Takeuchi, S. (1990). *Phys. Rev. Lett.* **65**, 1603–1605.

Yamamoto, A., Matsuo, Y., Yamanoi, T., Tsai, A. P., Hiraga, K. & Masumoto, T. (1995). *Aperiodic '94*, edited by G. Chapuis & W. Paciorek, pp. 393–398. Singapore: World Scientific.

Yamamoto, A. & Weber, S. (1997). *Phys. Rev. Lett.* **79**, 861–864.